TOXICOLOGICAL SCIENCES **128(2)**, 461–470 (2012)
doi:10.1093/toxsci/kfs171
Advance Access publication May 12, 2012

The Threshold Length for Fiber-Induced Acute Pleural Inflammation: Shedding Light on the Early Events in Asbestos-Induced Mesothelioma

Anja Schinwald,* Fiona A. Murphy,* Adriele Prina-Mello,† Craig A. Poland,‡ Fiona Byrne,§ Dania Movia,† James R. Glass,¶ Janet C. Dickerson,¶ David A. Schultz,¶ Chris E. Jeffree,‖ William MacNee,* and Ken Donaldson*,‡,[1]

**MRC/University of Edinburgh, Centre for Inflammation Research, Queen's Medical Research Institute, 47 Little France Crescent, Edinburgh EH16 4TJ, United Kingdom; †School of Medicine and Centre for Research on Adaptive Nanostructures and Nanodevices (CRANN), Trinity College Dublin, Dublin 2, Ireland; ‡Institute of Occupational Medicine, Research Avenue North, Riccarton, Edinburgh EH14 4AP, United Kingdom; §School of Physics and CRANN, Trinity College Dublin, Dublin 2, Ireland; ¶Seashell Technology, LLC,3252 Holiday Court, Suite 115, La Jolla, California 92037; and ‖University of Edinburgh, Institute of Molecular Plant Sciences, Daniel Rutherford Building, King's Buildings, Edinburgh EH9 3JH, United Kingdom*

[1]To whom correspondence should be addressed. Fax: 0131 651 1558. E-mail: ken.donaldson@ed.ac.uk.

Received February 10, 2012; accepted May 01, 2012

Suspicion has been raised that high aspect ratio nanoparticles or nanofibers might possess asbestos-like pathogenicity. The pleural space is a specific target for disease in individuals exposed to asbestos and by implication of nanofibers. Pleural effects of fibers depends on fiber length, but the key threshold length beyond which adverse effects occur has never been identified till now because all asbestos and vitreous fiber samples are heterogeneously distributed in their length. Nanotechnology advantageously allows for highly defined length distribution of synthetically engineered fibers that enable for in-depth investigation of this threshold length. We utilized the ability to prepare silver nanofibers of five defined length classes to demonstrate a threshold fiber length for acute pleural inflammation. Nickel nanofibers and carbon nanotubes were then used to strengthen the relationship between fiber length and pleural inflammation. A method of intrapleural injection of nanofibers in female C57Bl/6 strain mice was used to deliver the fiber dose, and we then assessed the acute pleural inflammatory response. Chest wall sections were examined by light and scanning electron microscopy to identify areas of lesion; furthermore, cell–nanowires interaction on the mesothelial surface of the parietal pleura *in vivo* was investigated. Our results showed a clear threshold effect, demonstrating that fibers beyond 4 μm in length are pathogenic to the pleura. The identification of the threshold length for nanofiber-induced pathogenicity in the pleura has important implications for understanding the structure–toxicity relationship for asbestos-induced mesothelioma and consequent risk assessment with the aim to contribute to the engineering of synthetic nanofibers by the adoption of a benign-by-design approach.

Key Words: **silver nanowires; asbestos; pleural inflammation; HARN; fiber threshold; risk assessment.**

Asbestos caused and continues to cause a pandemic of lung and pleural disease due to inhalation of airborne respirable fibers, which reach the most peripheral parts of the lungs producing fibrosis and lung cancer and enter the pleura causing fibrosis and mesothelioma (Delgermaa *et al.*, 2011; Heintz *et al.*, 2010; Mossman *et al.*, 2011). Because of these risks, asbestos has been banned in most Western countries but, due to exposure in the past and the long lag time to diagnosis, there is a substantial number of ongoing deaths from mesothelioma per year in countries that used asbestos industrially. High aspect ratio nanomaterials (HARN) are characterized by their high ratio of length to width, are nanoscale in two dimensions, may be made from a wide range of elements and compounds, and fall either into the category of nanotubes, nanowires, or nanorods (Donaldson *et al.*, 2011). Chrysotile asbestos fibrils, which are commonly less than 100 nm in diameter, fulfill the criteria for a HARN, albeit a naturally occurring example. The fibrous shape brings advantages over compact nanoparticulate counterparts for certain industrial applications, and the intrinsic size, shape, and properties of metal nanoparticles can be tailored and fine tuned with great precision (Wiley *et al.*, 2005). The increasing use of HARN in the nanotechnology industries inevitably implies increased risk of exposure of workers during manufacturing processes. This has attracted the attention of risk assessors and toxicologists due to the similarities between asbestos and HARN, with mesothelioma being a major focus of concern.

We previously recorded that direct exposure of the peritoneal (Poland *et al.*, 2008) and the pleural mesothelial surfaces (Murphy *et al.*, 2011) produced inflammatory and fibrotic effects only with long (>10 μm) samples of carbon nanotubes (CNTs), a manufactured nanofiber that is in ever-higher production. Crucially, this length-dependent effect is also seen with asbestos fibers in the induction of mesothelioma, lung cancer, and fibrosis in rats (Davis *et al.*, 1986). These studies clearly imply that long, straight CNT should be risk managed like asbestos (British Standards Institution, 2007).

© The Author 2012. Published by Oxford University Press on behalf of the Society of Toxicology. All rights reserved.
For permissions, please email: journals.permissions@oup.com

Downloaded from https://academic.oup.com/toxsci/article/128/2/461/1650273 by guest on 20 March 2024

A fiber pathogenicity paradigm has been developed based on toxicology studies with asbestos and other natural and man-made fibers (Donaldson *et al.*, 2009, 2011). In 1996, Kane summarized parameters that render a fibrous material pathogenic, that is, biopersistence, dimensions (length, width), chemical composition, and surface reactivity. The parietal pleura is the key site of retention of long, biopersistent fibers, and the pleura is a site where fiber-specific pathology, including pleural effusion and the mesothelioma, is initiated (Donaldson *et al.*, 1989, 2010). Studies investigating the role of the length of asbestos and other fibers *in vitro* and *in vivo* in the development of pleural disease led to the overwhelming conclusion that longer fibers (> approximately 8 µm) are more pathogenic than shorter fibers (Davis *et al.*, 1986; Davis and Jones, 1988; Dodson *et al.*, 2003; Heintz *et al.*, 2010). Although fiber length is accepted as the major contributing factor to fiber pathogenicity, the length threshold value at which long-fiber effects occur in the pleura is unknown.

In the present study, we utilized the technical advances of nanotechnology to produce nanofibrous structures in tightly defined length categories to investigate the threshold length for fiber effects in the pleural space.

MATERIALS AND METHODS

Particle panel. The panel of nanowires consisted of five different lengths of silver nanowires (AgNWs) (www.seashelltech.com), abbreviated in the text as $AgNW_3$, $AgNW_5$, $AgNW_{10}$, $AgNW_{14}$, and $AgNW_{28}$ according to their mean length in micrometer (µm). The AgNW panel was provided in isopropanol at a concentration of 30 mg/ml. They were synthesized using a polyol process as described in U.S. patent number 7,922,787 B2 issued to Seashell Technology, San Diego, CA. Synthesis of AgNW and reaction conditions to obtain different lengths did not affect the chemical composition of the different nanowires. Sizing of the nanowire length was performed by light microscopy (100× magnification using QCaptur objective) (n = 100) (Table 1 and Supplementary figs. 1A–C). Mixed length amosite asbestos enriched for long fibers (100% fibers ≥ 5 µm, 50.3% fibers > 15 µm, and 35.2% fibers > 20 µm), hereafter referred to as long fiber asbestos (LFA), and shortened amosite asbestos (SFA; 3.1% fibers ≥ 5 µm) (Donaldson *et al.*, 1989) were used to link the response to asbestos pathogenicity. Both LFA and SFA were created from the same batch of South African amosite (Davis *et al.*, 1986) obtained from the Manville Corporation, United States. SFA was prepared by grinding long fibers in a ceramic ball mill, and the resulting fiber preparation sedimented in water. The process of ball milling used to shorten the LFA to make the SFA was associated with small changes in the iron chemistry (Graham *et al.* 1999; Tomatis *et al.* 2010). SFA contained a consistent fraction of nonfibrous particles based on the definition of a fiber by the WHO (1997) (i.e., longer than 5 µm, thinner than 3 µm, and with an aspect ratio greater than 3:1). Additionally short (4 µm/$NiNW_4$) and long (20 µm/$NiNW_{20}$) nickel nanowires (NiNWs) and short (2 µm/NT_2) and long (13 µm/NT_{13} and 36 µm/NT_{36}) multiwalled CNTs (MWCNTs) were used (see Supplementary table 1 and Supplementary fig. 2) as alternative forms of HARN. (NiNWs) were fabricated by electrochemical template synthesis at Trinity College (TCD, Ireland) as previously reported by Byrne *et al.* (2009) and Poland *et al*. (forthcoming) (see Supplementary table 1). The surface of these wires is coated with a layer of nickel oxide, which is approximately of 3–4 nm thickness, which act as protective layer against the chemical dissolution (Prina-Mello *et al.*, 2006). Material particulate control panel consisted of Ag-nanoparticle (Ag-P), Ni-nanoparticle (Ni-P), nanoparticle carbon black (NPCB) as reported in Supplementary table 1. Nanowires were tested for the presence of bacterial endotoxins using a Limulus Amebocyte Lysate test (Lonza Group, Switzerland), but no endotoxin was detectable (detection limit < 10pg/ml). To test the endotoxin levels, supernatant of the AgNW and NiNW solutions were used to avoid interference of AgNW or NiNW with the assay.

Experimental animals. Nine-week-old female C57Bl/6 strain mice (Harlan, U.K.) were used in this study. Mice were kept in a group size of five in standard caging with sawdust bedding within a pathogen-free Home Office approved facility. Mice were maintained on a normal 12-h light and dark cycle. Prior to the treatment, mice were kept for 7 days in the facility to acclimatize. The work was carried out by staff holding a valid U.K. Home Office personal licence under a Home Office approved project licence.

TABLE 1
Characterization of Silver Nanowire Length (AgNW)

	$AgNW_3$	$AgNW_5$	$AgNW_{10}$	$AgNW_{14}$	$AgNW_{28}$
Mean length (µm)	3	5	10	14	28
% fiber per length category (µm)					
0.5–1.5	6	2	0	0	0
1.5–2.5	39	7	0	2	0
2.5–3.5	53	22	2	2	0
3.5–4.5	2	14	0	0	0
4.5–5.5		12	3	0	0
5.5–6.5		40	9	0	0
6.5–7.5		2	4	2	0
7.5–8.5		1	4	2	0
8.5–9.5			24	23	0
9.5–10.5			14	14	0
10.5–15.5			34	17	22
15.5–20.5			6	26	13
20.5–30.5				12	20
30.5–40.5					31
40.5–50.5					9
50.5–60.5					5
Diameter (nm, mean ± SEM)	115 ± 3	118 ± 3	128 ± 2	121 ± 3	120 ± 4

Downloaded from https://academic.oup.com/toxsci/article/128/2/461/1650273 by guest on 20 March 2024

Intrapleural injection and lavage. Samples were prepared in 0.5% bovine serum albumin (BSA; Sigma-Aldrich, Poole, U.K.)/saline and injected into the pleural cavity of unanesthetized female C57BI/6 mice at a dose of 5 µg per mouse and an injection volume of 100 µl per mouse. The site of injection was the right upper quadrant of the thorax. Mice were euthanized after 24 h and 1 week ($n = 4$) by asphyxiation in 100% CO_2. The pleural space was lavaged with three 1-ml washes of sterile saline. Cellular fraction and lavage fluid were separated by centrifugation. Total cell count was performed using a NucleoCounter (ChemoMetec, 7 A/S, Allerød, Denmark), and cyto-centrifugation followed by Diff-Quik staining using Diff-Quik stainset (Dade Behring GmbH, Marburg, Germany) were performed for differential cell counts. Images of lavaged cells were taken using QCapture Pro (Media Cybernetics Inc., Bethesda, MD).

Dissection. After 24-h and 1-week exposure, the lower right posterior portion of the chest wall was resected from the mice after lavage, washed in ice-cold saline, and fixed for 4 h in 30% formalin. The resected chest wall was an area of approximately 10 mm × 10 mm adjacent to the spine including the lower six ribs and intercostal space and, according to Shinohara *et al.* (1997), resulted to be rich in stomata. The chest wall was excised from the surrounding tissue, embedded on edge in paraffin, sectioned, and stained with hematoxylin and eosin for gross pathology ($n = 2$ per treatment for chest wall). Representative images of chest wall samples and lesion area were obtained by taking serial images at 10× magnification using QCapture Pro software (Media Cybernetics Inc.).

Scanning electron microscopy and backscatter secondary electron microscopy. Specimens were fixed and dehydrated as above, mounted on scanning electron microscopy (SEM) aluminum stubs, and rotary coated with about 8 nm of carbon in an Edwards 306A vacuum coating system (Edwards High Vacuum, Crawley, U.K.).

SEM of carbon-coated specimens was carried out using a Hitachi 4700 II field emission SEM (Hitachi High-Tech, Maidenhead, U.K.) at a beam accelerating voltage of 10 kV and a working distance of about 8 mm. Secondary electron (SE) and backscatter secondary electron (BSE) images were taken simultaneously using an annular YAG crystal BSE detector and the upper SE detector to produce perfectly synchronized image pairs. The two images were superimposed using Adobe Photoshop (Adobe Systems Incorporated, San Jose, CA) by layering the BSE image with the grayscale SE image using the Lighten function and pasting this image into the red channel of the SE image after conversion to RGB, thus color coding in red the strong BSE signal from the nanowires and the SE image appearing in gray.

Statistics. All data are shown as the mean ± SEM and these were analyzed using one-way analysis of variance. Multiple comparisons were analyzed using Tukey's honestly significant difference method and in all cases, values of $p < 0.05$ were considerably significant (GraphPad InStat Software Inc., La Jolla, CA).

RESULTS

Characteristics of the Particle Panel

AgNWs were characterized by SEM and light microscopy and showed a uniform dispersion in diameter and tight length distribution for each class (Table 1 and Supplementary fig. 1). Dissolution of AgNW was measured via change in pH compared with that of vehicle control across the 24-h exposure. No significant change in dissolution of AgNW occurred as shown by the almost flat slope of the curve across the 24-h exposure, and no difference in dissolution was observed between all AgNW lengths (Supplementary fig. S3A).

In addition to the AgNW panel, a range of nanofiber controls were used in this study including short (2 µm/NT_2) (mean length/acronym) and long (13 µm/NT_{13}, 36 µm/NT_{36}) MWCNTs (Murphy *et al.*, 2011) and short (4 µm/$NiNW_4$) and long (20 µm/$NiNW_{20}$) NiNWs. The CNT samples have been previously characterized by Murphy *et al.* (2011), whereas NiNWs were characterized according to their length distribution and diameter as previously described by Poland *et al.* (forthcoming) and Byrne *et al.* (2009), respectively. A modest extent of NiNW dissolution over 24 h was detected using pH change measurement; this is possible due to the saline solution degradation as shown by its reference curve (Supplementary fig. 3B).

Silver nanoparticulate (35 nm/Ag-P), NPCB, and Ni-P were included as material nanoparticulate controls. Well-characterized mixed length amosite asbestos enriched for long fibers and SFA (see Supplementary Information) were used as long (> 10 µm) and short pathogenic fiber control.

Acute Inflammatory Response to Intrapleural Injection of Silver Nanofibers and Controls

The pleural cavity was lavaged 24 h after intrapleural injection, and the acute inflammatory reaction measured as the total cell number and total granulocytes (predominantly neutrophils plus a low proportion of eosinophils) in the lavage. There was a clear length-dependent inflammatory response to AgNW, with significant increases in both total cell and total granulocyte number after treatment with AgNW that were 5 µm and longer (Figs. 1B and 1C) and LFA (Fig. 1D). In contrast, neither the very short fibers ($AgNW_3$ and SFA) nor the compact nanoparticles (Ag-P) elicited a significant inflammation (Figs. 1B–D). The length-dependent response reveals that the total granulocyte number induced was significantly increased ($p < 0.01$) with $AgNW_5$ compared with $AgNW_3$ (Fig. 1C). Moreover, there was no significant difference in inflammatory response (granulocytes) as length increased among $AgNW_5$, $AgNW_{10}$ and $AgNW_{14}$, demonstrating an all-or-nothing type of response beyond the 5 µm length. For $AgNW_{28}$, there was a significant increase in total cell number and granulocyte cell number compared with $AgNW_5$ (Figs. 1B and 1C). This all-or-nothing response was confirmed by a dose effect series for $AgNW_3$ and $AgNW_5$ (see Supplementary figs. 4A and 4B). $AgNW_3$ did not lead to a significant increase in inflammatory cells up to a tested dose of 10 µg per mouse.

The general design of this study used equal fiber mass; therefore, many more short fibers than long fibers were injected, yet still this greater number of short fibers in the dose of $AgNW_3$ was much less inflammogenic than the fewer long fibers in the dose of $AgNW_5$. Because fiber exposure is regulated in workplaces on the basis of the fiber number, we calculated the number of fibers per treatment for $AgNW_3$ and $AgNW_5$, the key lengths spanning the threshold value (see Supplementary materials and methods). Based on fiber number calculations, we reexpressed the inflammatory response 'per fiber,' and this

Downloaded from https://academic.oup.com/toxsci/article/128/2/461/1650273 by guest on 20 March 2024

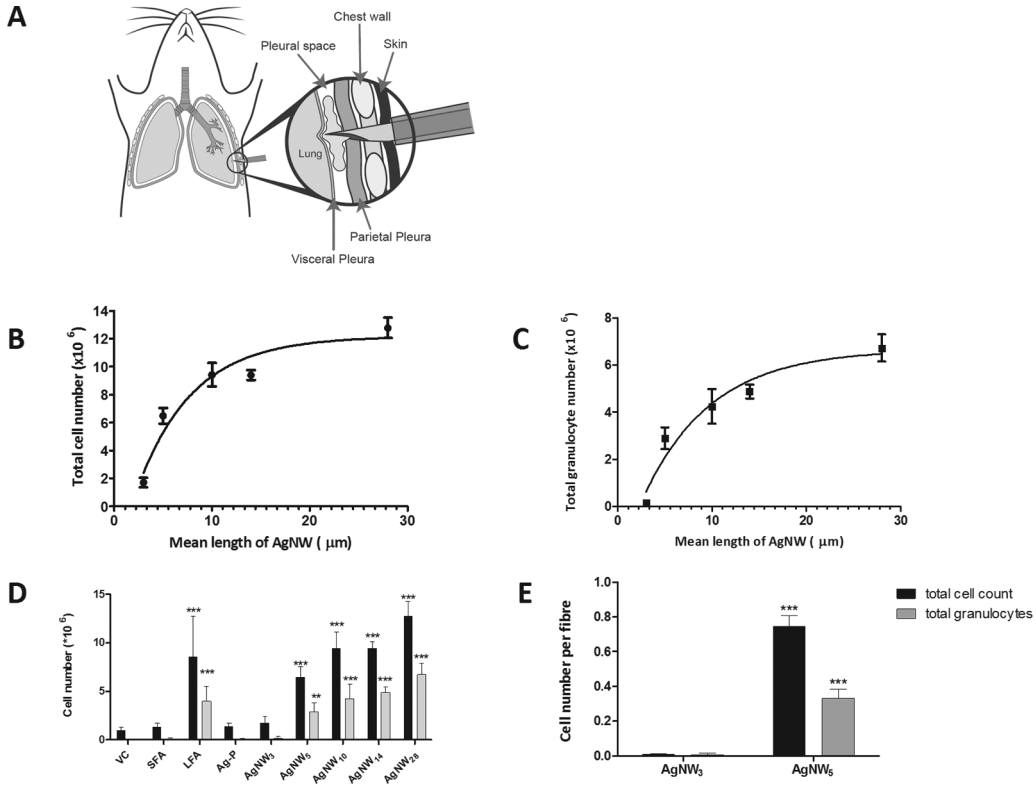

FIG. 1. Illustration of pleural injection and length-dependent response to AgNW in the pleural space 24 h postinjection. (A) Illustration of pleural injection showing a modified needle with a sleeve penetrating the chest wall into the pleural space to deliver the dose of nanofibers (Murphy *et al.*, 2011). (B) Count of total cell number in relation to fiber length of AgNW after 24-h treatment in female C57Bl/6 mice. All lengths were significantly greater than $AgNW_3$ ($p < 0.001$). Significant difference of $AgNW_5$ versus $AgNW_{10}$ ($p < 0.05$), $AgNW_5$ versus $AgNW_{14}$ ($p < 0.05$) and $AgNW_5$ versus $AgNW_{28}$ ($p < 0.001$) is observed. Data represent mean ± SEM of $n = 4$ mice. (C) Total granulocyte count from pleural lavage 24 h postinjection of AgNW in female C57Bl/6 mice. The influx of total granulocytes (neutrophil and eosinophil) is dependent on fiber length of AgNW. All lengths were significantly greater then $AgNW_3$ ($p < 0.01$–0.001). No significant difference of $AgNW_5$ versus $AgNW_{10}$ and $AgNW_5$ versus $AgNW_{14}$ is observed, whereas there is a significant difference of $AgNW_5$ versus $AgNW_{28}$ ($p < 0.001$). (D) Total cells and total granulocytes were counted in lavage fluid of mice treated with SFA, LFA, and AgNW panel. (E) Acute inflammatory response expressed per fiber. Equalization to fiber number reinforced the identified threshold value. Data represent mean ± SEM of $n = 4$ mice.

clearly showed that the fiber-specific inflammatory potency of the $AgNW_3$ fibers is negligible compared with the marked specific inflammogenicity of $AgNW_5$ fibers (Fig. 1E).

Light Microscopy and SEM of Parietal Pleura Surface

The pathogenic response to AgNW by the surface of the parietal pleura was examined by light microscopy and by SEM at 24-h postexposure. The pleural surface layer was a continuous normal mesothelium after intrapleural injection of vehicle control, SFA, Ag-P, and $AgNW_3$ (Figs. 2A–D). In contrast, sections of the parietal pleura from mice injected with LFA and $AgNW_{5/10/14/28}$ showed large lesions comprising macrophages and granulocytes at the pleural surface (Figs. 2E–I and Supplementary fig. 5).

Inflammatory Response After 7-Day Exposure

To address the course of the response, a 7-day time point was assessed at the 5-µg dose. The acute inflammatory response had largely resolved at this time point, although there was still a length-dependent effect detectable at $AgNW_{14/28}$ (Supplementary fig. 6A). Histological sections of the chest wall at 7 days continued to show thickening of the submesothelial cell layer in the same length-dependent pattern as the acute inflammation, that is, with a threshold at 5 µm (see Supplementary fig. 6B). BSE microscopy of *in vivo* biopersistence and light microscopy of *in vitro* durability showed that AgNWs retain their structural integrity over the 1-day time point but are not biopersistent over a protracted time (Fig. 3 and Supplementary fig. 7).

Phagocytosis of AgNW in Pleural Lavage Fluid and in Lesions on the Parietal Pleura

The degree of phagocytosis of different lengths of AgNW in pleural macrophages was assessed by light microscopy in cytospin preparations and by BSE in lesions on the parietal pleura. $AgNW_3$ and $AgNW_5$ could, for the most part, be fully phagocytosed inside pleural macrophages recovered in the lavage fluid (Fig. 3B) and in lesions on the parietal pleura imaged by BSE (Fig. 3F) at 1 day. In contrast, $AgNW_{10/14/28}$ lead to frustrated phagocytosis in the pleural macrophages (Figs. 3C–E and 3G, Supplementary fig. 8).

Downloaded from https://academic.oup.com/toxsci/article/128/2/461/1650273 by guest on 20 March 2024

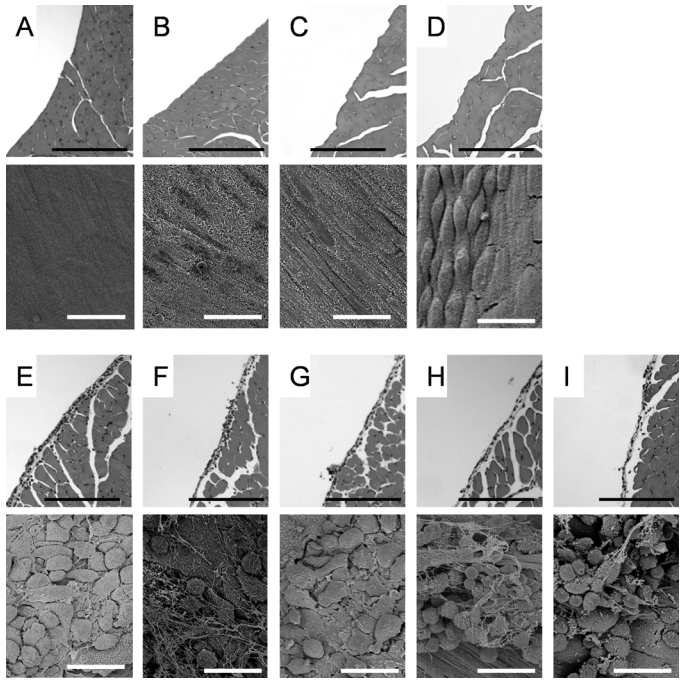

FIG. 2. Length-dependent response of AgNW on the parietal mesothelial surface 24 h postinjection. Hematoxylin and eosin histology sections and SEM images of VC (A), mice treated with Ag-P (B), $AgNW_3$ (C), SFA (D), $AgNW_5$ (E), $AgNW_{10}$ (F), $AgNW_{14}$ (G), $AgNW_{28}$ (H), and LFA (I). No alteration on the mesothelial surface can be seen in the mice treated with Ag-P, $AgNW_3$, and SFA. Normal mesothelial cells on the parietal pleura appear either flat as seen in the image of VC-exposed mesothelium or in a more rounded or raised form in areas called the lacunar regions, such as that seen in the image of SFA-exposed mesothelium (Donaldson *et al.*, 2010). Accumulation of inflammatory cells was observed on the mesothelial lining in mice treated with long AgNW (≥ 5 µm) and LFA. Scale bar: black 100 µm; white 20 µm.

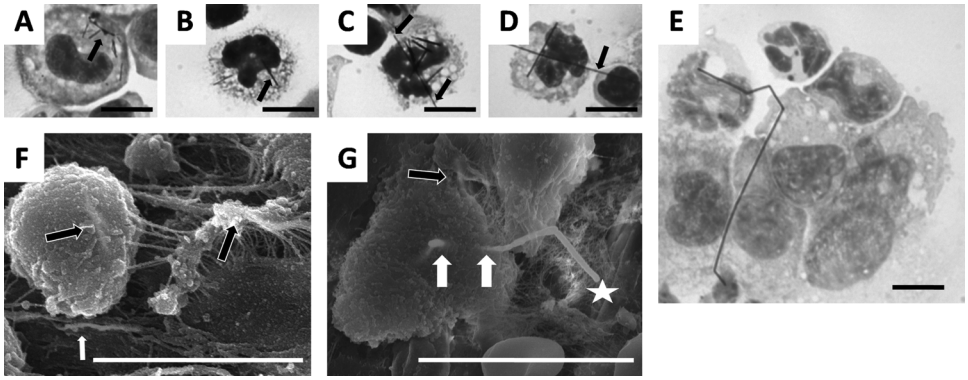

FIG. 3. Phagocytosis of AgNW in pleural lavage fluid and in inflammatory cells in lesions on the parietal pleura. Cytospin preparation of the pleural lavage fluid from mice treated with $AgNW_3$ (A) and $AgNW_5$ (B) shows complete phagocytosis of nanowires in pleural macrophages (nanowires indicated by the arrow). (C) $AgNW_{10}$ is not entirely phagocytosed, showing the ends of a nanowire protruding from a cell (indicated by two arrows). Frustrated phagocytosis of macrophages was observed after $AgNW_{14/28}$ treatment (D and E). A number of macrophages can be seen sharing a single fiber indicated by the arrow (F). All cytospin images are 100 magnification. Merged secondary electron and backscatter electron SEM images of the lesion's surface on the parietal pleura from mice treated with $AgNW_5$ (F) and $AgNW_{10}$ (G). (F) Two fibers are shown, which are fully phagocytosed by pleural macrophages (black arrows). The white arrow shows a fiber on the surface in the lesion area. (G) The star indicates frustrated phagocytosis of macrophages with $AgNW_{10}$. The loci where unclosed phagosomes must be present are indicated by the white arrows. The black arrow shows a fiber that is shared by two cells each of which must have an unclosed phagosome. Scale bar for all images 10 µm.

In addition, the presence of AgNW on the chest wall of mice treated with $AgNW_3$ was assessed, and no $AgNW_3$ could be found on the parietal pleura using BSE; hence, we assume that they were readily cleared from the pleural space after 24 h.

Role of Silver Ion Toxicity and Soluble Metals

We determined the release of soluble silver into saline for the different fiber lengths using inductively coupled plasma mass spectrometry, but these data are confounded by the formation

Downloaded from https://academic.oup.com/toxsci/article/128/2/461/1650273 by guest on 20 March 2024

of insoluble silver chloride. We also collected the soluble products from the AgNWs of long and short lengths into saline and assessed the ability to cause pleural inflammation. Although we found no difference between soluble extracts of short and long AgNWs, this also may have been confounded by the formation of silver chloride and so these data are not included in this paper. The issue of the potential formation of silver chloride from silver ions and chloride ions raises an important question as to whether silver ions could ever be toxic *in vivo* because of their rapid removal by the formation of insoluble silver chloride following reaction with chloride ions, which are ubiquitous in biological systems. Furthermore, it seems to be impossible to measure silver ion release from Ag-P into biological media because chloride ions would always be present in biological media with the formation of silver chloride.

Acute Inflammatory Response to Intrapleural Injection of Nickel Nanofibers, CNTs and Controls

The acute inflammatory response to AgNW and SFA/LFA in the pleural space after intrapleural injection was compared with other forms of HARN NT_2, NT_{13}, and NT_{36} (Murphy *et al.*, 2011) and $NiNW_4$ and $NiNW_{20}$ using the same method. NPCB and Ni-P were included as material nanoparticulate controls (Supplementary table S1). Particulates and short fibers (NPCB, Ni-P, Ag-P, SFA, NT_2, $AgNW_3$, $NiNW_4$) produced no significant increase in total cell number and granulocytes 24 h after intrapleural injection (Fig. 4). In contrast, all fiber samples that were 5 µm and longer produced an inflammatory response (LFA, NT_{13}, NT_{36}, $AgNW_{5/10/14/28}$, $NiNW_{20}$) (Fig. 4 and Supplementary fig. 9). The data clearly show that the threshold length for long fiber effects in the pleural space is 5 µm. The difference in response to $NiNW_4$ and $AgNW_5$ is dramatic but can be explained by their size distribution curves, which are illustrated in Figure 4B. Hardly any $NiNW_4$ are longer than 5 µm; however, ~40% $AgNW_5$ are ≥ 5 µm (see Supplementary figs. 1C and 2). Further information excluding a role for soluble Ni ions can be found in Supplementary Information.

Size of Stomata Across Mammalian Species

To link the outcome from the mouse study to the human risk relating to fiber length, the size of human parietal pleural stomata and the site of long fiber retention are most relevant. We performed a literature search on the size range of stomata on the diaphragm or the parietal pleura of various species, which shows a remarkable constancy (Table 2). From mouse to human, the size ranges from 0.8 to 10 µm. This is in agreement with allometric scaling for lung cells in mammals ranging in size from shrews to horses (Stone *et al.*, 1992), which showed no mean difference in size for cells such as epithelial cells across this large range of body mass.

DISCUSSION

In this study, the use of defined length classes of nanofibers allowed us to quantify the threshold length for inflammatory effects in the pleural space, the key site for fiber pathogenicity. A method of intrapleural injection of particles, previously described by Murphy *et al*. (2011), was used to measure acute inflammation in the pleural space. This method is justified on the basis that a fraction of all inhaled particles and fibers that deposit in the peripheral lung translocate into the pleural space (Mercer *et al.*, 2010; Miserocchi *et al.*, 2008; Mitchev *et al.*, 2002; Walton, 1982). A dose of 5 µg was selected to allow comparison of the results with previously published data investigating the length-dependent effect of CNT in the pleural space (Murphy *et al.*, 2011).

We used a very specific panel of AgNW in different length classes, otherwise identical in composition, diameter, and solubility. This demonstrated a clear length threshold value for fiber pathogenicity in the pleural space of 5 µm. Significant increase in total cell number and granulocytes in the pleural space was observed after exposure to fibers of a length including 5 µm and longer, which could be confirmed via histological and SEM examination of the parietal pleura of the chest wall. Injecting a single dose into the pleural space, as we have done here, massively overrepresents the number of fibers that reach the stomata compared with inhalation, yet there was no inflammatory effect of any of the short nanofibers. The fact that the huge dose and high dose rate of short fibers produced by instillation into the pleura proved noninflammatory argues that the short fibers would be noninflammatory to the pleura following inhalation, when the dose reaching the pleura and the dose rate to the pleura would be vastly less than used here.

In our previous study (Poland *et al.*, 2008), we emphasized the role of long fiber frustrated phagocytosis but had no data on the exact cutoff length. Here nanofibers in tight size ranges enabled us to show that true frustrated phagocytosis, where fibers actually protrude from the surface of the cell, is not necessary for long fiber-induced inflammation in the pleural space. This is argued on the basis that $AgNW_5$ caused inflammation in the pleural space but was for the most part phagocytosed by pleural macrophages.

The role of Ag ion in mediating the toxic effects of compact Ag-P has been discussed extensively. Information about the role of Ag ion release in observed toxicity of silver particulates is mainly based on *in vitro* experiments at extremely high doses and cannot be correlated with *in vivo* observations (Johnston *et al.*, 2010). Recent studies could not identify a significant health effect after nanosilver exposure in *in vivo* studies (Stebounova *et al.*, 2011). This is consistent with the primary role for fiber length in the pleural pathogenicity of the AgNW panel used here. If soluble silver was the explanatory factor for the pattern of inflammation after intrapleural AgNW injection, a greater amount of soluble Ag release from longer AgNW should be observed. This was shown not to be the case and in

Downloaded from https://academic.oup.com/toxsci/article/128/2/461/1650273 by guest on 20 March 2024

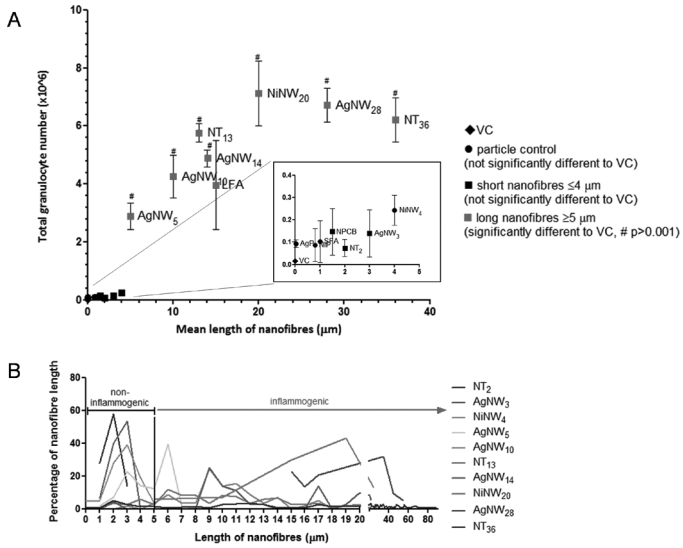

FIG. 4. The acute pleural response to CNT, NiNW, AgNW, SFA, and LFA in various lengths. (A) Female C57Bl/6 mice were intrapleurally instilled with 5 µg/mouse of NPCB (14 nm), NT_2, NT_{13}, NT_{36}, Ni-P, $NiNW_4$, $NiNW_{20}$, Ag-P (35 nm), $AgNW_3$, $AgNW_5$, $AgNW_{10}$, $AgNW_{14}$, $AgNW_{28}$, SFA, and LFA. Total granulocyte number is shown from pleural lavage 24-hour postexposure. A clear length-dependent threshold response in the pleural space to different sources and compositions of high aspect ratio nanomaterials from 5 µm in length is evident; NPCB/NT_2/NT_{36} data are obtained from Murphy *et al.* (2011). Length is shown as mean. Data represent mean ± SEM of $n = 4$ mice. (B) The percentage of nanofibers per length is plotted to illustrate their length distribution in relation to the cutoff length for fiber-induced pleural inflammation.

TABLE 2
Size of Stomata Across Mammalian Species

Species	Stomatal size (µm)	Reference
Bat	0.8–2	Azzali (1999)
Hedgehog, gerbil, bat, mouse	1.8–6	Azzali (1999)
Monkey	3–8	Oya *et al.* (1993)
Sheep	1–3	Lai-Fook (2004)
Human	6.2	Li (1993)
Rat, mouse, rabbit, hamster, human	4–10	Abu-Hijleh *et al.* (1995)
Human	2–8	Muller *et al.* (2002)

fact all samples give off negligible amounts of silver ions or other contaminating metals in femto- to picogram dilutions that would not be biologically active.

We set out to determine whether length was a unifying factor in pleural toxicity across a range of HARN in addition to AgNW to rule out material-specific effects and to further determine the length threshold for pleural inflammation. We obtained good support for the contention that, for acute pleural inflammation, length is the predominant structural explanatory variable across a range of fibrous nanomaterials and asbestos.

The greater pathogenic potency of long asbestos fibers in asbestos-induced pathology was identified in animal studies in the first half of the 20th century and with special reference to mesothelioma in the later studies of Stanton and Wrench (1972) and Davis *et al.* (1986). A mechanistic basis for the extra pathogenic effect of long asbestos fibers is evident in the greater retention of long fibers in the lungs compared with short fibers and the greater potency of long fibers in general at eliciting proinflammogenic effects *in vivo* (Poland *et al.*, 2008) and *in vitro* (Poland *et al.*, forthcoming). With special reference to the translocation of fibers to the pleural space and the occurrence of pleural pathology, we have noted that a fraction of all deposited particles translocate to the pleural space (Mercer *et al.*, 2010; Ryman-Rasmussen *et al.*, 2009). By using the model of direct pleural instillation, we bypassed various mechanisms of fiber clearance throughout the respiratory tract. However, recently, rodent pharyngeal aspiration and inhalation models using CNT (Mercer *et al.*, 2011; Ryman-Rasmussen *et al.*, 2009) verified the translocation of inhaled CNT to subpleural region where they caused pleural inflammation. However, so far the length threshold for fibers to reach the pleural space after inhalation exposure in rodent model is not known. Studies investigating the dimensions of asbestos fibers in mesothelial tissue from mesothelioma patients revealed that fibers up to a length of 62 µm were found in tumor tissue, with an average of 4.55 µm (Suzuki and Yuen, 2002). These data show that even the longest AgNW used in this study could potentially reach the subpleural tissue in humans after inhalation exposure. Nanofibers could reach the pleural space freely or in macrophages. In the study by Ryman-Rasmussen *et al*. (2009), MWCNTs were found subpleurally in macrophages, in subpleural mesenchymal cells, and free in the collagen matrix of the subpleura. In the study by Mercer *et al*. (2011), the "pleural penetrations" of CNT could be free fiber or fibers in macrophages. Long fibers translocated to the pleural space, both free or inside macrophages, are retained because they cannot negotiate the stomata in the parietal pleura, through which the efferent flow

Downloaded from https://academic.oup.com/toxsci/article/128/2/461/1650273 by guest on 20 March 2024

of pleural fluid passes (Donaldson *et al.*, 2010). We believe that this explains the propensity of long fibers to cause pleural effects including mesothelioma when compact particles and short fibers do not. However, till this point, there has been no quantitative data on the threshold length for retention at the parietal stomata. The data here suggest that fibers of 5 µm, and above in length, are likely to be retained at the stomata where they can elicit inflammation. However, we do not doubt that a high enough dose of the shorter fibers would be inflammogenic in the pleural cavity due to artifactual aggregation into mats and clog in the stomata. This was shown previously by Kane (1996) in the peritoneal cavity, which possesses identical stomatal mechanism for fiber clearance (Goodglick and Kane, 1990).

Naturally, for purposes of extrapolating to the human risk relating to fiber length, the size of human parietal pleural stomata and the site of long fiber retention are most relevant. Across mammalian species, there is a remarkable consistency in the reported size of stomata on the diaphragm or parietal pleura. Therefore, we suggest that our findings of a general threshold for fiber retention that is applicable to humans are well served by the mouse model described here. We can only speculate on the events that follow from the first retention of a long fiber at a stoma, but the lodging of a long fiber at a stoma and recruitment of inflammatory cells to it may enhance the likelihood of further retention of long fibers and lead eventually to effective blockage of the stoma.

It has not escaped our notice that the global regulation of fibers is based on a standard definition of a fiber as an object that has a length greater than 5 µm, a width less than 3 µm, and an aspect ratio of greater than 3:1 (WHO, 1997). The 5-µm length regulatory standard was defined in the middle of the last century, and its origin was described in 1982 by Walton (Walton, 1982). It is fortuitous that the length of 5 µm was chosen, albeit without recourse to any scientific knowledge on length-dependent parietal pleural retention, as a margin of safety from long fibers (10–20 µm) that were known, even then, to be the most pathogenic fraction (Walton, 1982).

Ours is of course a study of a short-term response, but we contend that it is rationally related to long-term pathology in the pleural space and the argument for this is twofold. The first is the argument of dose, by which we mean that the model we put forward relies on acute inflammation as both a marker of, and a response to, retention in the pleural space and we confirm here that short fibers transit out of the pleural space. So long fibers must represent the only dose that could be related to the acute, but importantly also the chronic, responses seen in the pleural space to fibers. The second argument is based on the endpoint studied: inflammation is known to be directly related to fibrosis and cancer caused by asbestos through well-understood pathways and mechanisms (Dai and Churg, 2001; Dostert *et al.*, 2008; Nagai and Toyokuni, 2010; Unfried *et al.*, 2002).

The fact that the AgNWs used here were not biopersistent beyond a few days and does not detract from the relevance of the length-dependent effects demonstrated here. Biopersistent fibers of the same dimensions would have the same acute effect as AgNWs but, in contrast, would evoke an ongoing chronic inflammatory response that would lead to pathological change as we have reported for long, biopersistent MWCNTs (Murphy *et al.*, 2011). A clear link therefore exists between fiber length and the potential to cause acute inflammation; additionally, there is a link between fiber biopersistence and the ability for acute inflammation to become chronic and a link between chronic pleural inflammation and the common pleural pathologies associated with asbestos exposure, such as pleural fibrosis and mesothelioma.

Biopersistence therefore remains a key factor in determining the pathogenic effects of long nanofibers and warrants further elucidation, if the biopersistent nanofibers in narrowly defined length classes similar to the AgNW can be obtained. Our data suggest that any long, biopersistent fiber will be retained on the parietal pleura and is likely to engender chronic inflammation.

The conclusion of the threshold length of this study is mainly based on linear, straight, single fibers. However, long fibers that are tangled and agglomerated in their overall morphology, as is often the case with tangled CNT, have been shown to cause less inflammation due to their tightly packed spherical agglomerated state (Murphy *et al.*, 2011; Poland *et al.*, 2008). Therefore, the aggregation state of the nanofibers has to be considered to assess their toxicity.

In summary, our data provide for the first time a quantitative threshold for respirable fiber length in inducing pleural inflammation using a range of nanofibers. The threshold length for inducing pleural inflammogenicity in a range of fibers including amosite asbestos is 5 µm in the mouse, which we suggest can be extrapolated to humans. This knowledge is a valuable addition to our understanding of the mechanism of asbestos-related pleural disease, especially for mesothelioma and its relationship to fiber length. We recognize that this research was carried out in a mouse model and with a necessarily restricted range of nanofibers and that extrapolation to humans is not straightforward. Therefore, for regulatory purposes, we urge further research on the important issue of the threshold length for safe fibers with regard to the mesothelioma hazard to the pleura and the role of biopersistence. From the present data, however, we may conclude that, for acute inflammation, there is good evidence that short fibers less than 5 µm in length form the basis of safer-by-design nanofibers, and this has an important implication for fiber and nanofiber risk assessment.

SUPPLEMENTARY DATA

Supplementary data are available online at http://toxsci.oxfordjournals.org/.

FUNDING

Colt Foundation (A.S., K.D.); the Department of Health (F.A.M.); NAMDIATREAM (EU-FP7 project ref 246479

Downloaded from https://academic.oup.com/toxsci/article/128/2/461/1650273 by guest on 20 March 2024

to A.P.-M., F.B.); CRANN Pathfinder (Science Foundation Ireland CSET programme to D.M.).

ACKNOWLEDGMENTS

We thank S. Mitchell (University of Edinburgh) for sample preparation for SEM and technical assistance.

REFERENCES

Abu-Hijleh, M. F., Habbal, O. A., and Moqattash, S. T. (1995). The role of the diaphragm in lymphatic absorption from the peritoneal cavity. *J. Anat.* **186**(Pt 3)**,** 453–467.

Azzali, G. (1999). The lymphatic vessels and the so-called "lymphatic stomata" of the diaphragm: A morphologic ultrastructural and three-dimensional study. *Microvasc. Res.* **57,** 30–43.

British Standards Institution. (2007). *PD 6699-2:2007 Guide to safe handling and disposal of manufactured nanomaterials*. Available at http://www.bsigroup.com/en/sectorsandservices/Forms/PD-6699-2/Download-PD6699-2-2007/. Accessed June 20, 2012.

Byrne, F., Prina-Mello, A., Whelan, A., Mohamed, B. M., Davies, A., Gun'ko, Y. K., Coey, J. M. D., and Volkov, Y. (2009). High content analysis of the biocompatibility of nickel nanowires. *J. Magn. Magn. Mater.* **321,** 1341–1345.

Dai, J., and Churg, A. (2001). Relationship of fiber surface iron and active oxygen species to expression of procollagen, PDGF-A, and TGF-beta(1) in tracheal explants exposed to amosite asbestos. *Am. J. Respir. Cell Mol. Biol.* **24,** 427–435.

Davis, J. M., Addison, J., Bolton, R. E., Donaldson, K., Jones, A. D., and Smith, T. (1986). The pathogenicity of long versus short fibre samples of amosite asbestos administered to rats by inhalation and intraperitoneal injection. *Br. J. Exp. Pathol.* **67,** 415–430.

Davis, J. M., and Jones, A. D. (1988). Comparisons of the pathogenicity of long and short fibres of chrysotile asbestos in rats. *Br. J. Exp. Pathol.* **69,** 717–737.

Delgermaa, V., Takahashi, K., Park, E. K., Le, G. V., Hara, T., and Sorahan, T. (2011). Global mesothelioma deaths reported to the World Health Organization between 1994 and 2008. *Bull. World Health Organ.* **89,** 716–724C.

Dodson, R. F., Atkinson, M. A., and Levin, J. L. (2003). Asbestos fiber length as related to potential pathogenicity: A critical review. *Am. J. Ind. Med.* **44,** 291–297.

Donaldson, K., Brown, G. M., Brown, D. M., Bolton, R. E., and Davis, J. M. (1989). Inflammation generating potential of long and short fibre amosite asbestos samples. *Br. J. Ind. Med.* **46,** 271–276.

Donaldson, K., Murphy, F., Schinwald, A., Duffin, R., and Poland, C. A. (2011). Identifying the pulmonary hazard of high aspect ratio nanoparticles to enable their safety-by-design. *Nanomedicine (Lond).* **6,** 143–156.

Donaldson, K., Murphy, F. A., Duffin, R., and Poland, C. A. (2010). Asbestos, carbon nanotubes and the pleural mesothelium: A review of the hypothesis regarding the role of long fibre retention in the parietal pleura, inflammation and mesothelioma. *Part. Fibre Toxicol.* **7,** 5

Dostert, C., Petrilli, V., Van, B. R., Steele, C., Mossman, B. T., and Tschopp, J. (2008). Innate immune activation through Nalp3 inflammasome sensing of asbestos and silica. *Science* **320,** 674–677.

Goodglick, L. A., and Kane, A. B. (1990). Cytotoxicity of long and short crocidolite asbestos fibers in vitro and in vivo. *Cancer Res.* **50,** 5153–5163.

Graham, A., Higinbotham, J., Allan, D., Donaldson, K., and Beswick, P. H. (1999). Chemical differences between long and short amosite asbestos: Differences in oxidation state and coordination sites of iron, detected by infrared spectroscopy. *Occup. Environ. Med.* **56,** 606–611.

Heintz, N. H., Janssen-Heininger, Y. M., and Mossman, B. T. (2010). Asbestos, lung cancers, and mesotheliomas: From molecular approaches to targeting tumor survival pathways. *Am. J. Respir. Cell Mol. Biol.***42,** 133–139.

Johnston, H. J., Hutchison, G., Christensen, F. M., Peters, S., Hankin, S., and Stone, V. (2010). A review of the in vivo and in vitro toxicity of silver and gold particulates: Particle attributes and biological mechanisms responsible for the observed toxicity. *Crit. Rev. Toxicol.* **40,** 328–346.

Kane, A. B. (1996). Mechanisms of mineral fibre carcinogenesis. *IARC Sci. Publ.* **140**, 11–34.

Lai-Fook, S. J. (2004). Pleural mechanics and fluid exchange. *Physiol. Rev.* **84,** 385–410.

Li, J. (1993). Ultrastructural study on the pleural stomata in human. *Funct. Dev. Morphol.* **3,** 277–280.

Mercer, R. R., Hubbs, A. F., Scabilloni, J. F., Wang, L., Battelli, L. A., Friend, S., Castranova, V., and Porter, D. W. (2011). Pulmonary fibrotic response to aspiration of multi-walled carbon nanotubes. *Part. Fibre Toxicol.* **8,** 21.

Mercer, R. R., Hubbs, A. F., Scabilloni, J. F., Wang, L., Battelli, L. A., Schwegler-Berry, D., Castranova, V., and Porter, D. W. (2010). Distribution and persistence of pleural penetrations by multi-walled carbon nanotubes. *Part. Fibre Toxicol.* **7,** 28.

Miserocchi, G., Sancini, G., Mantegazza, F., and Chiappino, G. (2008). Translocation pathways for inhaled asbestos fibers. *Environ. Health* **7,** 4.

Mitchev, K., Dumortier, P., and De, V. P. (2002). 'Black Spots' and hyaline pleural plaques on the parietal pleura of 150 urban necropsy cases. *Am. J. Surg. Pathol.* **26,** 1198–1206.

Mossman, B. T., Lippmann, M., Hesterberg, T. W., Kelsey, K. T., Barchowsky, A., and Bonner, J. C. (2011). Pulmonary endpoints (lung carcinomas and asbestosis) following inhalation exposure to asbestos. *J. Toxicol. Environ. Health B Crit. Rev.* **14,** 76–121.

Muller, K. M., Schmitz, I., and Konstantinidis, K. (2002). Black spots of the parietal pleura: Morphology and formal pathogenesis. *Respiration* **69,** 261–267.

Murphy, F. A., Poland, C. A., Duffin, R., Al-Jamal, K. T., Ali-Boucetta, H., Nunes, A., Byrne, F., Prina-Mello, A., Volkov, Y., Li, S., *et al.* (2011). Length-dependent retention of carbon nanotubes in the pleural space of mice initiates sustained inflammation and progressive fibrosis on the parietal pleura. *Am. J. Pathol.* **178,** 2587–2600.

Nagai, H., and Toyokuni, S. (2010). Biopersistent fiber-induced inflammation and carcinogenesis: Lessons learned from asbestos toward safety of fibrous nanomaterials. *Arch. Biochem. Biophys.* **502,** 1–7.

Oya, M., Shimada, T., Nakamura, M., and Uchida, Y. (1993). Functional morphology of the lymphatic system in the monkey diaphragm. *Arch. Histol. Cytol.* **56,** 37–47.

Poland, C. A., Byrne, F., Cho, W. S., Prina-Mello, A., Murphy, F. A., Davies, G. L., Coey, J. M., Gounko, Y., Duffin, R., Volkov, Y., *et al.* (Forthcoming). Length-dependent pathogenic effects of nickel nanowires in the lungs and the peritoneal cavity. *Nanotoxicology*.

Poland, C. A., Duffin, R., Kinloch, I., Maynard, A., Wallace, W. A., Seaton, A., Stone, V., Brown, S., MacNee, W., and Donaldson, K. (2008). Carbon nanotubes introduced into the abdominal cavity of mice show asbestos-like pathogenicity in a pilot study. *Nat. Nanotechnol.* **3,** 423–428.

Prina-Mello, A., Diao, Z., and Coey, J. M. (2006). Internalization of ferromagnetic nanowires by different living cells. *J. Nanobiotechnol.* **4,** 9.

Ryman-Rasmussen, J. P., Cesta, M. F., Brody, A. R., Shipley-Phillips, J. K., Everitt, J. I., Tewksbury, E. W., Moss, O. R., Wong, B. A., Dodd, D. E., Andersen, M. E., *et al.* (2009). Inhaled carbon nanotubes reach the subpleural tissue in mice. *Nat. Nanotechnol.* **4,** 747–751.

Shinohara, H. (1997). Distribution of lymphatic stomata on the pleural surface of the thoracic cavity and the surface topography of the pleural mesothelium in the golden hamster. *Anat. Rec.* **249,** 16–23.

Downloaded from https://academic.oup.com/toxsci/article/128/2/461/1650273 by guest on 20 March 2024

Stanton, M. F., and Wrench, C. (1972). Mechanisms of mesothelioma induction with asbestos and fibrous glass. *J. Natl. Cancer Inst.* **48,** 797–821.

Stebounova, L. V., Mcakova-Dodd, A., Kim, J. S., Park, H., O'Shaughnessy, P. T., Grassian, V. H., and Thorne, P. S. (2011). Nanosilver induces minimal lung toxicity or inflammation in a subacute murine inhalation model. *Part. Fibre Toxicol.* **8**, 5.

Stone, K. C., Mercer, R. R., Gehr, P., Stockstill, B., and Crapo, J. D. (1992). Allometric relationships of cell numbers and size in the mammalian lung. *Am. J. Respir. Cell Mol. Biol.* **6,** 235–243.

Suzuki, Y., and Yuen, S. R. (2002). Asbestos fibers contributing to the induction of human malignant mesothelioma. *Ann. N.Y. Acad. Sci.* **982,** 160–176.

Tomatis, M., Turci, F., Ceschino, R., Riganti, C., Gazzano, E., Martra, G., Ghigo, D., and Fubini, B. (2010). High aspect ratio materials: Role of surface chemistry vs. length in the historical "long and short amosite asbestos fibers". *Inhal. Toxicol.* **22,** 984–998.

Unfried, K., Schürkes, C., and Abel, J. (2002). Distinct spectrum of mutations induced by crocidolite asbestos: Clue for 8-hydroxydeoxyguanosine-dependent mutagenesis in vivo. *Cancer Res.* **62,** 99–104.

Walton, W. H. (1982). The nature, hazards and assessment of airborne dust: A review. *Ann. Occup. Hyg.* **25,** 117–247.

Wiley, B., Sun, Y. G., Mayers, B., and Xia, Y. N. (2005). Shape-controlled synthesis of metal nanostructures: The case of silver. *Chem.-A Eur. J.* **11,** 454–463.

WHO. (1997). *Determination of Airborne Fiber Number Concentration: A Recommended Method by Phase Contrast Microscopy.* WHO, Geneva, Switzerland.

Downloaded from https://academic.oup.com/toxsci/article/128/2/461/1650273 by guest on 20 March 2024